Journal of ELECTRONIC MATERIALS, Vol. 46, No. 11, 2017
DOI: 10.1007/s11664-017-5680-9

A Fast Responsive Ultraviolet Sensor from mSILAR-Processed Sn-ZnO

DEEPU THOMAS,[1,5] K.A. VIJAYALAKSHMI,[2] KISHOR KUMAR SADASIVUNI,[3] AJITH THOMAS,[1] DEEPALEKSHMI PONNAMMA,[4] and JOHN-JOHN CABIBIHAN[3]

1.—Research and Development Centre, Bharathiar University, Coimbatore 641046, India. 2.—Department of Physics, Sri Vasavi College, Erode 638 316, India. 3.—Department of Mechanical and Industrial Engineering, Qatar University, P.O. Box 2713, Doha, Qatar. 4.—Center for Advanced Materials, Qatar University, P.O. Box 2713, Doha, Qatar. 5.—e-mail: deepuskariankal@gmail.com

Microwave-assisted successive ionic layer adsorption and reaction was employed to synthesize Sn-ZnO (tin-doped zinc oxide), and its sensitivity to ultraviolet radiation is compared with zinc oxide (ZnO). The sensing films were made by the dip-coated method on an indium titanium oxide glass substrate, and the sensing performance was monitored using the 300–700 nm wavelength of UV–Vis light. Excellent sensitivity and recovery were observed for the Sn-doped ZnO sensor device, especially at 380 nm wavelength of ultraviolet (UV) light (response and recovery time 2.26 s and 8.63 s, respectively, at 5 V bias voltage). The variation in photocurrent with respect to dark and light illumination atmosphere was well illustrated based on the Schottky and inter-particle network effects. Doping of Sn on ZnO nanoparticles varied the surface roughness and crystallite size as observed from scanning electron microscopic and x-ray diffraction studies. Here, we demonstrate a simple and economical fabrication technique for designing a high-performance UV light sensor. The developed device works at room temperature with high durability and stability.

Key words: Electronics, mSILAR, doping, metal nanoparticles, optical sensor

INTRODUCTION

Ultraviolet (UV) light is an electromagnetic spectral region with a lower wavelength than visible light (10–400 nm). For live animals, this radiation is a double-edged sword, and it possesses numerous good applications as well as harmful effects. The beneficial applications of UV light include polymer degradation, photography, photolithography, fire detection, optical sensors, fluorescent dyes, photovoltaics, etc. The direct irradiation of UV light can cause harmful effects to the eyes and skin. For UV radiation, sensors are very significant as far as the electronic industry is concerned. The areas where UV sensors find applications include automobiles, printing, robotics, pharmaceuticals, production transportation of chemicals and so on.[1,2] Conventional sensors used to detect UV radiation and based on semiconductors (silicon, galium nitride, etc.) have shortcomings and a low sensitivity for detecting the visible and Infrared radiation (IR) regions. Also, additional filters are needed, and thus the set-up involves a complicated design.[3,4]

Electronic and optoelectronic devices strongly influence the current industrial technologies. Extensive research has been focused on the properties and potential applications of nanomaterials.[5–10] Recently, nano-ZnO has emerged out as one of the most favorable materials for electronics, piezoelectrics, spintronics, solar cells and sensing

(Received November 25, 2016; accepted July 6, 2017; published online July 20, 2017)

applications. ZnO is an *n*-type semiconductor having a high band gap (3.37 eV) and exhibiting good magnetic, optical, and electrical properties. It possesses high optical gain and strong responsivity, high chemical stability, scalable device fabrication methods, easy synthesis and comparatively low cost.[6–9] This nanomaterial has been widely reported on for its capability for detecting UV light.[11–14] Highly sensitive UV light switches were made using one-dimensional ZnO particles by Kind et al.,[15] whereas a photoconductive UV detector was made by laterally growing ZnO.[16] The influence of the processing conditions on the response to UV light for ZnO nanowires has been well investigated.[17–19] Chai et al. developed UV detectors based on naturally self-assembled crossed ZnO nanorods.[18] Furthermore, doping of ZnO offers the fabrication of UV photodetectors having different cut-off wavelengths by adjusting the band gap.[10,20] Moreover, the photocurrent responses of crystalline ZnO grown on flexible substrates has been analyzed under various UV intensities.[21] Three-dimensional nanowires and nanorods of ZnO were grown by Gao et al. using the high-temperature solid vapor deposition method and they obtained ultra-responsive sensing.[22] Similar to these studies, in situ generation of ZnO nanoparticles in different dimensions by means of several simple and low-cost techniques have been reported for making UV detectors with faster responses. However, mechanical robustness, biocompatibility, high quality and quantity production, etc. are the most desirable characteristics for broader applications. There are many UV detectors available in the current market, especially quick response silicon-based photo sensors having very high sensitivity and low noise. Though Si-based detectors exhibit a quicker response compared to ZnO-based devices, the latter stands out from the former for its high selectivity and ultra-high vacuum condition, as well as not requiring a high voltage.[23] The wide band gap and the ability to operate under harsh environmental conditions are additional advantages of this material.[24]

The essential conditions for a material to be ideally UV responsive include high sensitivity, quick response and maximum durability. ZnO sensors have disadvantages like slow recovery and responses are often observed due to the adsorption/desorption of oxygen (hole trapping) occurring during the photoresponsive process.[25–27] The band gap of ZnO can be tuned to the desired value by doping with various elements, and can make UV sensors for different cut-off wavelengths.[20,32] The sensing ability of ZnO has been studied in both undoped and doped forms. Tin (Sn) is an active *n*-type dopant in metal oxides especially ZnO, and it is favorable for substituting Zn ions in ZnO to form a Sn-ZnO lattice due to the radius of Zn^{+2} (0.074 nm) being almost equal to Sn^{+4} (0.071 nm). Ates et al.[29] fabricated humidity sensors based on Sn-doped ZnO with low Sn contents, and found that there is an increase in humidity sensing with doping. Hendi et al.[32] also fabricated a humidity sensor based on ZnO and Sn-doped ZnO (Sn used 0.5 at.% and 4 at.%) and measured the sensing behavior by using a quartz crystal microbalance at low frequency.

In the present study, a simple fabrication strategy has been adopted for the synthesis of ZnO and Sn-ZnO nanoparticles. Microwave-assisted successive ionic layer adsorption and reaction (mSILAR) is an established technique for nanoparticle synthesis. Using this method, Sn-ZnO was deposited on indium titanium oxide (ITO) glass to investigate the photoresponsivity. Normal morphology characterizations revealed that the exact structural information of the material is the spheroidal shape (<40 nm diameter). The major focus of this work is to fabricate a sensor by a simple synthesis method and UV response of the sensor at a wavelength of 380 nm. Various parameters such as sensitivity, response time, recovery time, etc. were determined. It is aimed to design an effective and fast optoelectronic sensor based on Sn-ZnO and thus to contribute towards flexible electronics and photoelectronic devices made from semiconductor oxide.

EXPERIMENTAL

Materials

The chemicals, zinc sulfate heptahydrate ($ZnSO_4{\cdot}7H_2O$), sodium hydroxide (NaOH) and stannic (IV) chloride pentahydrate ($SnCl_45H_2O$) were obtained from Merck. Ultra-pure water (<18.2 MΩ cm) from the Milli-Q-Plus system (Millipore) was used to prepare aqueous solutions. All chemicals purchased were AR grade and used without further purification.

Fabrication of Sn-ZnO Sensors

ZnO and Sn-ZnO were deposited on ITO glass substrates (20 mm × 20 mm) by mSILAR.[30] Initially, an ITO glass electrode was fabricated by a lithography process. The ITO glass surface was cleaned and covered by a photo-resistant dry film. Then, it was illuminated by UV using a lamp and covered with an electrode mask. The ITO film of the developed substrate was fully covered with photo-resistant (Kapton) tape except for the active region. After UV irradiation, the photo-resist was developed. The prepared sample was immersed in an etching solution (HNO_3 and HCl in 1:10 ratio) to eliminate the ITO from the other part of the electrode. For further cleaning, it was placed in an ultrasonic bath in a cleansing agent (soap) solution and, subsequently, de-ionized water, isopropyl alcohol, and acetone for 10 min. Two electrical contacts were made from the exposed ITO of both sides of the active layer. The prepared ITO electrode was dipped in sodium zincate by using a prompt microcontrolled dip-coating unit at 90–95°C and the process was

repeated 100 times. Similarly, the Sn-doped ZnO was synthesized by adding $SnCl_4{\cdot}5H_2O$ to the sodium zincate bath and mixing with a magnetic stirrer at constant stirring speed. The atomic percentage $y = [Sn^{4+}]/[Zn^{2+}] = 5\%$ of the Sn dopant in the ZnO-based film was used. After the sample preparation, the Kapton tape was peeled off, and the ZnO active layer (14 mm × 14 mm) covering the electrode etched area remained. Finally, the obtained dip-coated films were annealed at 450°C in ambient conditions using a heat-annealing chamber.

Characterization Methods

The morphology of the Sn-ZnO sample was analyzed by atomic force microscopy (AFM) (diCaliber Veeco AFM) and field emission scanning electron microscopy (FE-SEM; JEOL, JSM-6460LV SEM). JA EM 3010 was used to capture high-resolution transmission electron microscope (TEM) images of the samples. The optical absorbance of the material was tested by an ultraviolet–visible (UV–vis) spectrophotometer (UV Pharmaspec 17000; Shimadzu). The crystalline structure was investigated by powder x-ray diffraction (XRD) experiments (Bruker AXS-8 using CuKα radiation). Electrical contacts were made on the electrode to analyze the current–voltage characteristics using a Keithley 2100. Photoconductivity was tested using the Keithley 6485 pm at 365 nm photon wavelength and 1.4 mW/cm^2 power density. For all measurements, the area of the photodetectors exposed to the UV radiation was kept constant. The response and recovery time have also been recorded for both samples for comparison.

RESULTS AND DISCUSSION

Structural Characterization

The AFM image of the Sn-ZnO is shown in Fig. 1a. It is evident from the image that all the particles exhibit a uniform spherical morphology. The surface roughness of the Sn-ZnO particles was calculated using the Park system XEI analyzing software and found to be 181 nm. The thickness of the ZnO film measured by AFM was 300 nm. The change in grain size of the ZnO was observed by Sn doping. Figure 1b–d shows the SEM, the SEM of a cross-section of the film and TEM images of the synthesized Sn-ZnO nanomaterial. The average diameter of the particles ranges from 30 nm to 60 nm, and dense particles of similar geometries can be clearly observed. The thickness of the Sn-ZnO film is approximately ~300 nm (Fig. 1c), which is similar to that obtained from AFM. The HR-TEM image reveals the monocrystalline structure of the material with uniform particle size.

Figure 2a shows the powder XRD spectrum of the ZnO and Sn-ZnO samples. The main peaks observed corresponds to the (100), (101) and (002) planes of the ZnO crystalline structure, which is in accordance with the reported behavior.[31] These peaks were at 2θ values of 33°, 34.4° and 36.25°, respectively, for the (100), (002), and (101) planes. All these peaks originate from a wurtzite lattice and are indexed accordingly.[30] For the peak corresponding to the (002) plane, the full width half maximum value is about 0.15°. The crystalline size for Sn-ZnO was calculated according to Eq. 1.

$$D = \frac{0.9\lambda}{\beta_{hkl} cos\theta} \quad (1)$$

where D is the crystallite size, β_{hkl} is the peak width at half maximum intensity, θ is the diffraction angle, and λ is the wavelength of the x-ray. The crystal size of the Sn-ZnO sample was calculated to be 31.3 nm. From this value, it is clear that Sn doping decreases the ucleation rate, as the dopant particles are settled inside the ZnO lattice.[32] The lower rate of nucleation and growth of the pure ZnO nanoparticles corresponds to a reduction of the crystallite size. The XPS analysis was used to determine the Sn-ZnO formation by simple elemental analysis. Figure 2b displays the successful incorporation of Sn into ZnO and confirms the declared empirical formulas. It is evident that neither the ZnO or Sn-implanted ZnO samples have any XPS signals from alien impurities.

The optical absorption spectrum of Sn-ZnO in the 300–700 nm region is given in Fig. 2c, and large absorption is observed at 300 nm, which is related to ZnO by the reported results.[33] The synthesized ZnO was shown to have a similar size and characterization as that of the ZnO particles reported elsewhere.[31] A linear relationship between $(\alpha h\nu)^2$ and $h\nu$ is observed ($h\nu = A(h\nu - E_g)^{1/2}$; $h\nu$ photon energy, A constant, E_g optical band gap, α absorption coefficient) for both ZnO[30] and Sn-ZnO. The band gap was calculated as 3.29 eV and 3.3 eV for ZnO and Sn-ZnO, respectively. The red shift in the band gap is attributed to the increasing carrier concentration in Sn-ZnO due to Sn doping. Depending on the level of impurity doping, the band gap varies. This is due to the change in electronic transitions due to the presence of dopant impurities within the ZnO networks. A high percentage of dopant decreases the band gap to a great extent, and so optimum dopant levels are selected based on this value.[34]

UV Sensor Design and the Mechanism

A schematic representation of the sensor design is demonstrated in Fig. 3. Both the planar (Fig. 3a) and angled (Fig. 3b) views of the Sn-ZnO coated ITO glass plate are given. In short, the device design consists of an ITO-coated glass slide, (1) with an Sn-ZnO active layer, (2) a zigzag-shaped etched area on the ITO film, (3) which provides a strip of Sn-ZnO connecting two ITO electrodes (4 and 5). The width of the strip is around 1 mm. The ITO electrodes are contacted with

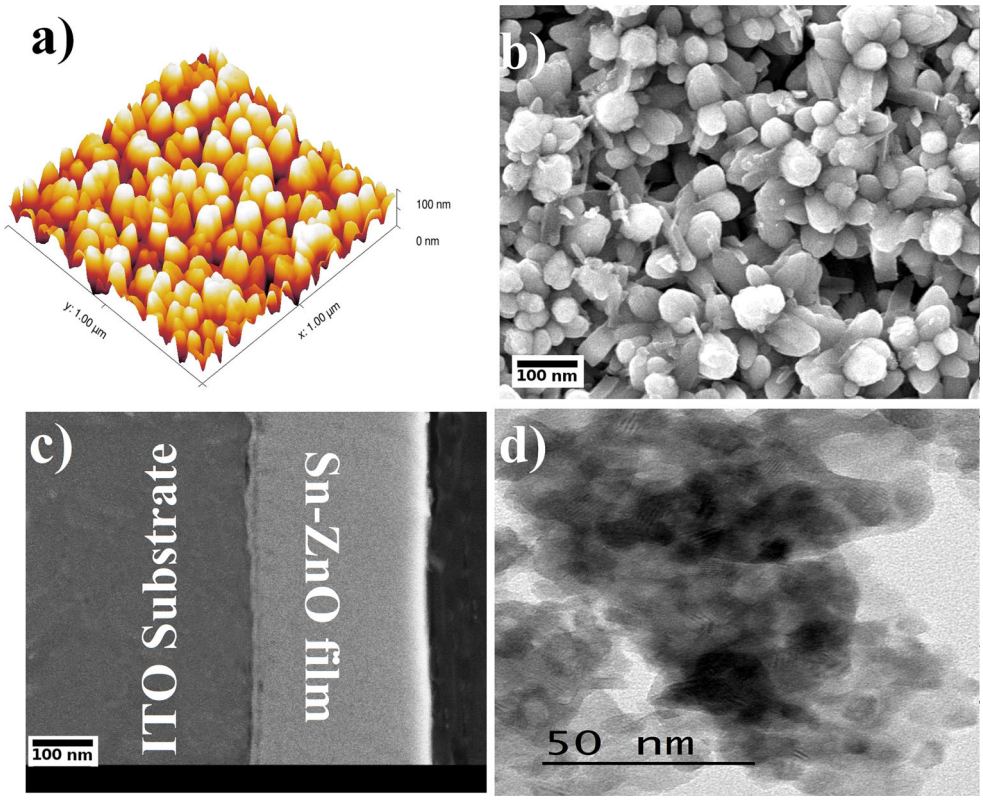

Fig. 1. (a) AFM, (b) FE-SEM, (c) FESEM (cross-section of film), and (d) TEM.

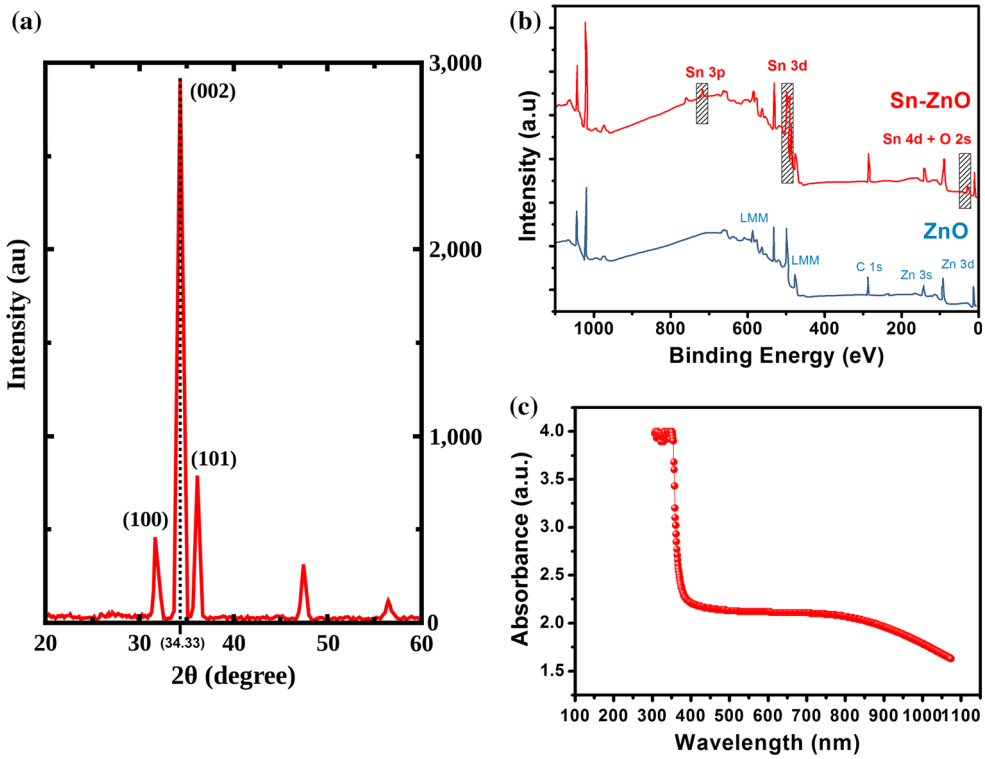

Fig. 2. (a) XRD analysis of Sn-ZnO, (b) XPS spectra for Sn-implanted ZnO and (c) UV–vis.

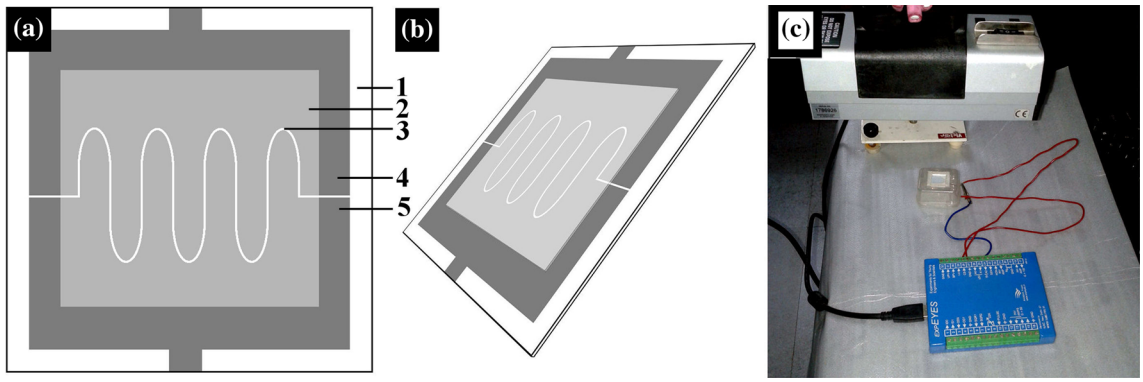

Fig. 3. (a) Planar and (b) angled views of the device, (c) experimental set-up.

Sn-ZnO strip longitudinally, and so the length of the active region becomes higher. The sensing performance of the Sn-ZnO sample material was tested by keeping the device under a 5-W UV lamp with a radiation area 31.5 cm^2 (7 cm × 4.5 cm) and intensity 0.159 W/cm^2. The experimental set-up for sensing is shown in Fig. 3. The sample connection set-up from the electrode is clearly shown in Fig. 3c. The screenshot with the help of EXPEYES (Experiments for young engineers and scientists) software was used to analyze UV sensing by monitoring the source voltage and current. The EXPEYES is a mode of characterization through which the device response and recovery time are checked. This software was employed for the purposes of a mini-digital oscilloscope, function generator, current source, voltage source, etc. by connecting it to a personal computer via a USB cable. The device was connected to a 5-V source, and it monitored the current from the sensor when UV light switching took place.

To start with, the whole device was kept in the dark for 5 s, and, thereafter, the UV light was exposed. The current–voltage (I–V) characteristics and the UV sensing performance of the Sn-ZnO are illustrated in Fig. 4. The current behavior of ZnO and Sn-ZnO was compared and plotted against time as shown in Fig. 4a. The efficiency of a sensor is determined from its response time and recovery time. The recovery time is defined as the time required for attaining the response back to the initial state after the UV light was cut off from the sensor, and the response time denotes the initial time required in generating a response after the UV radiation is exposed. The recovery times were calculated as 15.26 s and 8.63 s for ZnO and Sn-ZnO, respectively. Similarly, the response times of ZnO and Sn-ZnO were calculated to be 8.2 s and 2.26 s.

The results indicate that the response of the Sn-doped ZnO was significantly higher than that of the ZnO. The measured electrical conductivity also showed that the Sn-ZnO sensing layer exhibited a lower resistance compared to the ZnO film due to more conductive carriers or disorder in the ZnO lattice. The fast sensing behavior of Sn-ZnO was expected due to the particle network junctions and conduction channels arising out of the Schottky contacts. The point junctions created at the sensor surface and oxygen developed the potential barriers which cause the fluctuations in the output current.[35–39]

From the I–V curve (Fig. 4b), it is revealed that the current first rises and reaches saturation due to the decrease in the resistance of the Sn-ZnO sample. When saturation is attained, the UV source has been turned off to achieve recovery. The wavelength of 365 nm was used for UV radiation. Rectifying behaviors are observed for the I–V characteristics of the Sn-ZnO under light and dark illumination conditions. This behavior indicates the Schottky contacts at the Sn-ZnO interface, and the photocurrent/dark current ratio was increased with bias. Responses of the UV detector for cyclic illuminations are shown in Fig. 4c and d, which reveals the durability and stability of the sensor-based device. Here, the dark and photocurrent were measured at a 5-V bias voltage. About 2000 repeated cyclic simulations were recorded to confirm the durability of the sensor, and itwas is established that the Sn-ZnO sample exhibited excellent repeatability and durability.

The higher response time observed by the UV detector can be related to the charge transport behavior regulated by the inter-particle contacts. For each ZnO particle, there is a depletion region, and this acts as a barrier hindering the particle–particle electron transfer. Upon doping, the diameter of the ZnO particles changes and, ultimately, the diameter exceeds the Debye length and causes charge transport through the inter-particle junctions. The distance over which a local electric field disturbs the distribution of free charge carriers represents the Debye length or space–charge thickness. The space–charge layer is a region that has deficient carriers due to electron trapping by the chemisorbed oxygen. The electronic properties are more influenced by oxygen adsorption–desorption processes at the surface, and the Debye length also plays a major role in the properties variation.[36]

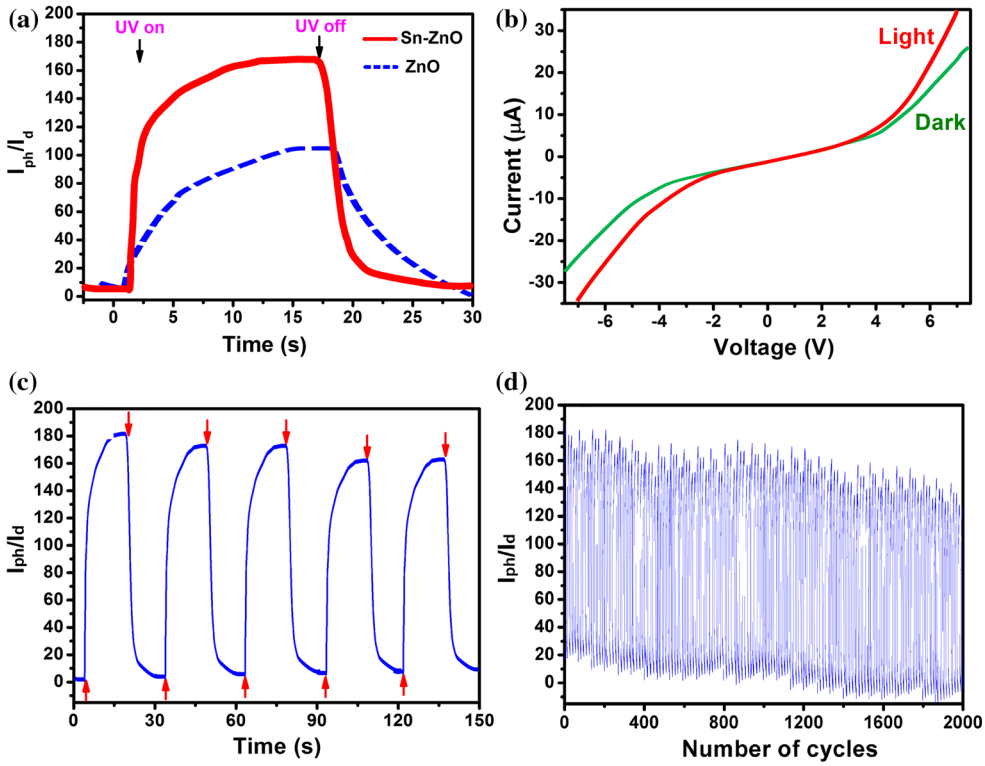

Fig. 4. (a) UV sensing analysis of ZnO and Sn-ZnO with their response and recovery times, (b) I–V curve of the Sn-ZnO sensor measured in the dark and under UV light, (c) Sn-ZnO sensor cyclic exposure, (d) durability and stability of the Sn-ZnO sensor under 50 cycles of exposure.

Figure 5a is a schematic representation of doped and undoped ZnO energy levels. The Sn-ZnO sensor absorbs the incident radiation when the photon energy is greater than the band gap energy E_g or E_{go}, and the re-adsorbed O_2^- would be discharged by producing the electron–hole pairs, as shown in Fig. 5b. The adsorption of oxygen molecules on the surface of the film and the capture of the free electrons present in the ZnO conduction band form O_2^{2-} and O_2^- when the Sn-doped ZnO film is exposed to air. A high depletion layer resistance near the surface of the ZnO will be formed in the presence of air during the process. The holes concentration will be lowered by h^+ recombining with e^- after the UV light is switched off, and the adsorbed oxygen molecules capture free electrons and thereby the conductance decreases (Sn-doped ZnO).[28] The following equations can express the main chemical reactions occurring.

$$O_2(g) + e^- \rightarrow O_2^-(ad)$$

$$O_2(g) + 2e^- \rightarrow O_2^{2-}(ad)$$

When the UV sensor is illuminated, the electron–hole (e^-–h^+) pairs are generated ($h\nu \rightarrow e^-$–h^+) and the holes discharge the chemisorbed oxygen ions. This process lowers the depletion layer thereby increasing the conductance.

$$O_2^-(ad) + h^+ \rightarrow O_2(g)$$

$$O_2^{2-}(ad) + 2h^+ \rightarrow O_2(g)$$

Alejandro et al. proposed that, when UV is exposed over the photoconductive surface, it releases oxygen desorption thereby initiating current fluctuations in the sensor that directly depend on the oxygen concentration around the sensor's surface.[37] This concept is strong evidence for the present work which states that sensitivity directly depends on the oxygen concentration.

The response and recovery times of our device were compared with the response and recovery times of other reported work (Table I). The superiority of our device is clear from the tabulated data. In this study, the first case sample was synthesized using the vapor phase transport and condensation (VPTC) method,[15] the second case by spray pyrolysis,[17] and the third and fourth cases by aqueous chemical growth (ACG) and sol–gel,[18,19] respectively. In addition, the mSILAR method employed in the present study is simple, exhibits faster response and recovery times and is economical. The technique also allows large area deposition of the sample compared to other methods. These properties make the fabricated device a highly selective visible–blind UV detector.

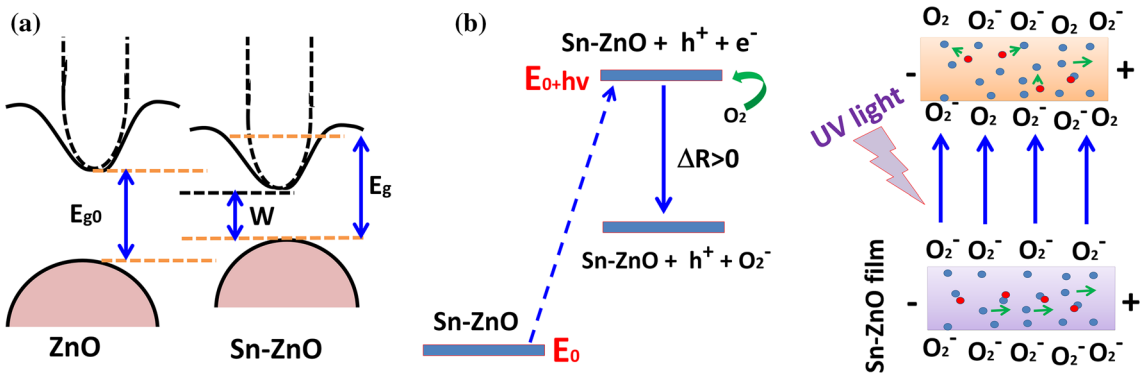

Fig. 5. Schematic band diagrams of (a) ZnO thin film and Sn-ZnO thin film (b) showing the mechanism for enhancing the UV sensing performance.

Table I. Comparison of ZnO UV sensors performance with reported work

Sample	Synthesizing method	Response time (s)	Decay time (s)	References
ZnO Nps	Spray pyrolysis	12	9	15
ZnO Nps	VPTC	13.9	398	17
ZnO Nws	ACG	10	62	18
ZnO nanorod arrays	Sol–gel	10	26	19
ZnO thin film	mSILAR	2.26	8.63	Present work

Nps Nanoparticles, *Nws* nanowires, *VPTC* vapor phase transport and condensation method, *ACG* aqueous chemical growth, *mSILAR* microwave-assisted successive ionic layer adsorption and reaction.

CONCLUSION

In summary, we have demonstrated the facile and cost-effective fabrication of a typical UV sensor using Sn-doped ZnO synthesized by mSILAR. The sensor characteristics such as response and recovery times under dark and UV light illuminations were investigated. The response time and recovery times of the fabricated device were found to be 2.26 s and 8.63 s, respectively. Alternatively, the fast switching ("ON" and "OFF") device makes it a high-quality photosensitive switch compared with other available devices. The proposed sensor can be scaled up to commercial UV detectors due to their growing interest and various uses. As a future work, we are planning to analyze the optimized concentration of Sn in Sn-ZnO for better sensitivity, and to observe the flexibility of the sensor in different environmental (humidity and temperature) conditions.

ACKNOWLEDGEMENT

This publication was made possible by the support of an NPRP grant from the Qatar National Research Fund (NPRP 7 - 673 - 2 - 251). The statements made here are solely the responsibility of the authors.

REFERENCES

1. E. Monroy, F. Calle, J.L. Pau, E. Muñoz, F. Omnès, B. Beaumont, and P. Gibart, *J. Cryst. Growth* 230, 537 (2001).
2. E. Monroy, F. Omnes, and F. Calle, *Semicond. Sci. Technol.* 18, R33 (2003).
3. S.J. Young, L.W. Ji, S.J. Chang, and Y.K. Su, *J. Cryst. Growth* 293, 43 (2006).
4. E. Munoz, E. Monroy, J.L. Pau, F. Calle, F. Omnes, and P. Gibart, *J. Phys. Condens. Matter* 13, 7115 (2001).
5. T.M. Barnes, J. Leaf, S. Hand, C. Fry, and C.A. Wolden, *J. Appl. Phys.* 96, 7036 (2004).
6. S. Goutham, D.S. Kumar, K.K. Sadasivuni, J.-J. Cabibihan, and K.V. Rao, *J. Electron. Mater.* 46, 2334 (2017).
7. S. Goutham, S. Kaur, K.K. Sadasivuni, J.K. Bal, N. Jayarambabu, D.S. Kumar, and K.V. Rao, *Mater. Sci. Semicond. Process.* 57, 110 (2017).
8. K. Deshmukh, M.B. Ahamed, R.R. Deshmukh, S.K.K. Pasha, K. Chidambaram, K.K. Sadasivuni, D. Ponnamma, and M.Al. AlMaadeed, *Polym. Plast. Technol. Eng.* 55, 1240 (2016).
9. K. Deshmukh, M.B. Ahamed, R.R. Deshmukh, S.K.K. Pasha, K.K. Sadasivuni, D. Ponnamma, and M. Al-Ali AlMaadeed, *J. Mater. Sci. Mater. Electron.* 28, 559 (2016).
10. A. Hezam, K. Namratha, Q.A. Drmosh, B.N. Chandrashekar, K.K. Sadasivuni, Z.H. Yamani, C. Cheng, and K. Byrappa, *Cryst.Commun. Eng.* (2017). doi:10.1039/C7CE00609H.
11. S.P. Ghosh, K.C. Das, N. Tripathy, G. Bose, D.H. Kim, T.I. Lee, J.M. Myoung, and J.P. Kar, *IOP Conf. Ser. Mater. Sci. Eng.* 115, 012035 (2016).
12. A.J. Gimenez, J.M. Yáñez-Limón, and J.M. Seminario, *J. Phys. Chem. C* 115, 282 (2011).
13. C.-H. Lin, S.-J. Chang, W.-S. Chen, and T.-J. Hsueh, *RSC Adv.* 6, 11146 (2016).
14. Z. Wang, R. Yu, X. Wang, W. Wu, and Z.L. Wang, *Adv. Mater.* 28, 6880 (2016).
15. H. Kind, H. Yan, B. Messer, M. Law, and P. Yang, *Adv. Mater.* 14, 158 (2002).
16. Y. Li, V.F. Della, M. Simonnet, and I. Yamada, *Nanotechnology* 20, 045501 (2009).

17. S. Dhara and P.K. Giri, *Nanoscale Res. Lett.* 6, 504 (2011).
18. G. Chai, O. Lupan, L. Chow, and H. Heinrich, *Sens. Actuators A* 150, 184 (2009).
19. L. Chow, O. Lupan, and G. Chai, *Phys. Stat. Sol. B* 247, 1628 (2010).
20. Th Gruber, C. Kirchner, R. Kling, F. Reuss, and A. Waag, *Appl. Phys. Lett.* 84, 5359 (2004).
21. J. Liu, W. Wu, S. Bai, Y. Qin, and A.C.S. Appl, *Mater. Interfaces* 3, 4197 (2011).
22. P.X. Gao, C.S. Lao, W.L. Hughes, and Z.L. Wang, *Chem. Phys. Lett.* 408, 174 (2005).
23. R.D. McKeag, S.S.M. Chan, and R.B. Jackman, *Appl. Phys. Lett.* 67, 2117 (1995).
24. Y.W. Heo, B.S. Kang, L.C. Tien, D.P. Norton, F. Ren, J.R.L. Roche, and S.J. Pearton, *Appl. Phys. A* 80, 497 (2005).
25. T.T. Pham, K.Y. Lee, J.H. Lee, K.H. Kim, K.S. Shin, M.K. Gupta, B. Kumar, and S.W. Kim, *Energy Environ. Sci.* 6, 841 (2013).
26. J.L. Hou, S.J. Chang, and S.P. Chang, *Int. J. Electrochem. Soc.* 8, 5650 (2013).
27. M.R. Alenezi, S.J. Henley, and S.R.P. Silva, *Sci. Rep.* 5, 8516 (2015).
28. S.I. Inamdar, V.V. Ganbavle, and K.Y. Rajpure, *Superlattices Microstruct.* 76, 253 (2014).
29. T. Ateş, C. Tatar, and F. Yakuphanoglu, *Sens. Actuators* 190, 153 (2013).
30. D. Thomas, S. Augustine, K.K. Sadasivuni, D. Ponnamma, J.J. Cabibihan, A.Y. Al Haddad, and K.A. Vijayalakshmi, *J. Electron. Mater.* 45, 1 (2016).
31. D. Thomas, S.C. Vattappalam, S. Mathew, and S. Augustine, *Adv. Chem.* 2014, 1 (2014).
32. A.A. Hendi, R.H. Alorainy, and F. Yakuphanoglu, *J. Sol–Gel Sci. Technol.* 72, 559 (2014).
33. A. Bedia, F.Z. Bedia, M. Aillerie, N. Maloufi, S. Ould Saad Hamady, O. Perroud, and B. Benyoucef, *Opt. Mater.* 36, 1123 (2014).
34. F. Yakuphanoglu, S. Ilican, M. Caglar, and Y. Caglar, *Superlattices Microstruct.* 47, 732 (2010).
35. D. Ponnamma, K.K. Sadasivuni, M. Strankowski, Q. Guo, and S. Thomas, *Soft Matter* 9, 10343 (2013).
36. K.K. Sadasivuni, A. Kafy, L. Zhai, H.U. Ko, S. Mun, and J. Kim, *Small* 11, 1002 (2015).
37. K.K. Sadasivuni, A. Kafy, H.C. Kim, H.-U. Ko, S. Mun, and J. Kim, *Synth. Met.* 206, 154 (2015).
38. K.K. Sadasivuni, D. Ponnamma, H.-U. Ko, H.C. Kim, L. Zhai, and J. Kim, *Sens. Actuators B Chem.* 233, 633 (2016).
39. D. Ponnamma, K.K. Sadasivuni, S. Thomas, I. Krupa, and M.A.A. AlMa'adeed, *Rubber Chem. Technol.* 89, 306 (2016).